Journal of Alloys and Compounds 485 (2009) 444–450

Contents lists available at ScienceDirect

Journal of Alloys and Compounds

journal homepage: www.elsevier.com/locate/jallcom

Characterization and reliability study of low temperature hermetic wafer level bonding using In/Sn interlayer and Cu/Ni/Au metallization

Da-Quan Yu[a,*], Chengkuo Lee[a,b], Li Ling Yan[a], Meei Ling Thew[a], John H. Lau[a]

[a] Institute of Microelectronics, A*STAR (Agency for Science, Technology and Research), 11 Science Park Road, Singapore Science Park II, Singapore 117685, Singapore
[b] Department of Electrical and Computer Engineering, National University of Singapore, 4 Engineering Drive 3, Singapore 117576, Singapore

ARTICLE INFO

Article history:
Received 4 April 2009
Received in revised form 27 May 2009
Accepted 28 May 2009
Available online 6 June 2009

Keywords:
WLP
Low-temperature bonding
In–Sn
Intermetallic compound
Hermeticity

ABSTRACT

Low temperature hermetic wafer bonding using In/Sn solder interlayer and Cu/Ni/Au metallization was investigated for microelectromechanical system (MEMS) packaging application. The thin Ni layer was used as a buffer layer to control the diffusion process between solder interlayer and Cu. Bonding was performed in a vacuum wafer bonder at 180 and 150 °C for 20 min with a pressure of 5.5 MPa. It was found that bonding at 180 °C, voids free joints composed of high temperature intermetallic compounds (IMCs) were obtained with good hermeticity. However, bonding at 150 °C, voids were generated along the seal joint which caused poor hermeticity comparing with that bonded at 180 °C. Four types of reliability tests, i.e., pressure cooker test, high humidity storage, high temperature storage and temperature cycling test were performed to evaluate the reliability of the seal joints bonded at 180 °C. In the failed dies, the propagation of crack along bonding line was found. The possible failure mechanism was discussed, and feasible improvement methods were proposed.

1. Introduction

Low-cost vacuum packaging of microelectromechanical system (MEMS) has become one of the most important challenges for successful commercialization of MEMS [1–4]. Wafer level bonding is a cost-effective method for MEMS packaging [5–7]. Recently low temperature wafer bonding process was driven by the MEMS manufacturing because dissimilar materials will result in a mechanical stress proportional with annealing temperature. In many MEMS devices, bonding of substrate with electronic structure is more and more used, and the use of metal electrical interconnects requires temperature below 400 °C [5]. Further, in some applications low processing temperature process is necessary for system integration. For example, image sensor module requires a relative low process temperature (below 200 °C) because it contains polymer structures like micro-lens which is sensitive to the temperature [8]. Various low temperature wafer bonding technologies have been investigated and they are categorized as two main approaches, i.e., direct bonding using special surface treatment techniques (such as plasma surface activated bonding [9], atom beam irradiation [10]) and intermediate layer bonding using polymers [11] and low temperature solders based on diffusion soldering method [12–23].

Diffusion soldering is a technique which can produce bonded joints at a moderate temperature that are subsequently stable at higher temperatures. Materials for diffusion soldering are composed of by two parts, i.e., solder combinations that contain low-melting-point (LMP) components such as In, and/or Sn, and high-melting-point (HMP) components such as Au, Ag, Cu, etc. The principle of diffusion soldering is the formation of homogeneous intermetallic compounds (IMCs) in the bonding process [24]. The applications of diffusion soldering technique in electronics packaging are like wafer level hermetic sealing [1,2,8,12–23] and three-dimensional (3-D) interconnects for 3-D stacked ICs (integrated circuits) or MEMS [24].

Materials systems like Sn/Au, In/Au, In/Ag, In/Cu and In/Sn have been investigated as diffusion soldering materials [11,15–25]. As aforementioned, lower bonding temperature is preferred. Bonding temperature is mainly determined by the melting point of LMP solder, e.g., In or Sn in the materials systems of Sn/Au, In/Au, In/Ag or In/Cu. Therefore, eutectic In–Sn alloy is a very attractive solder material for bonding because of its low eutectic temperature, i.e., 118 °C [22–23]. Since Cu is used widely as the interconnect material in advanced semiconductor industry and in modern packaging technology, and much cheaper comparing with Au, Cu is an appropriate HMP component for diffusion soldering in IC and MEMS industries.

For wafer level hermetic bonding, the total thickness variation (TTV) is a big issue, which is caused by wafer warpage and uneven surface due to materials deposition. This problem becomes severer when the wafer size increases from 4 to 8 in. or even larger. Suf-

* Corresponding author. Tel.: +65 67705429; fax: +65 67745747.
E-mail address: yudq@ime.a-star.edu.sg (D.-Q. Yu).

0925-8388/$ – see front matter © 2009 Elsevier B.V. All rights reserved.
doi:10.1016/j.jallcom.2009.05.136

ficient solder is required to reduce the effect of the non-planarity issue. Therefore, usually the bonding materials and bonding parameters for chip to chip bonding can not directly used to wafer to wafer boning. The reason lies that the TTV is smaller for a chip, and a thinner solder layer is suitable to get a good bonding. In our previous work [23], we have investigated 8 in. wafer to wafer bonding at 180 °C using In/Sn/Cu metallization. We found that solder material would be consumed before bonding when LMP solder was deposited directly on HMP component. This is the main root cause for low yield of good packaged dies and poor hermeticity issue. By introducing Ni buffer layer into the HMP components, 100% bonding yield was achieved at 180 °C with a bonding pressure of 5.5 MPa for 20 min [23]. The thin Ni buffer layer played a key role for the successful bonding by controlling the diffusion soldering process.

As aforementioned, lower bonding temperature is preferred in some MEMS applications. At the same time, for such thin IMC seal joint, long-term reliability is a concern when the sealed device or package is used under harsh environment such as high temperature, high humidity and so on. In this paper, 8 in. hermetic wafer bonding was performed at 180 or 150 °C. The effect of bonding temperatures on the microstructure, mechanical and hermetic properties of the seal rings was studied extensively. In addition, the reliability of such thin IMC joint was investigated in detail.

2. Experimental

2.1. Wafer fabrication and bonding process

8 in. wafers patterned with bonding rings and cavities were prepared. The schematic configuration of the cap wafer and bottom wafer for bonding is shown in Fig. 1(a). The square ring has the size of 11 mm × 11 mm and the width of 300 μm, while the V-groove cavity has the size of 6 mm × 6 mm and the depth of 250 μm. The cavity was formed by using wet-etching process with KOH inside of each bonding ring. Fig. 1(b) shows the multilayer structure of the solder/HMP interface of the bonding ring. At first, 300 Å thick SiO_2 and 1500 Å SiN were prepared on silicon wafer by thermal oxidation and low-pressure chemical vapor deposition (LPCVD). They acted as hard mask for cavity etching. The photolithography patterning process

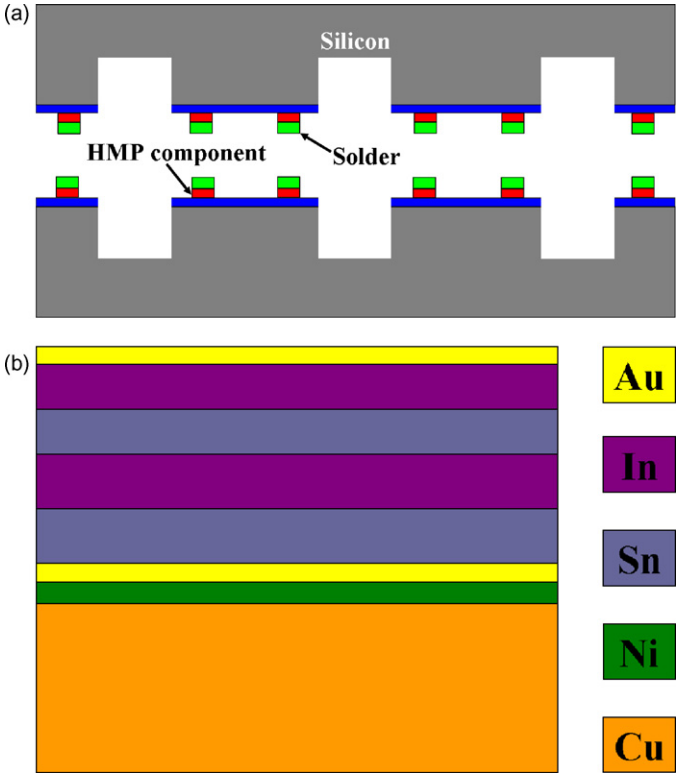

Fig. 1. Schematic configuration of (a) the cap wafer and the bottom wafer for bonding; (b) the multilayer structure of LMP/HMP components.

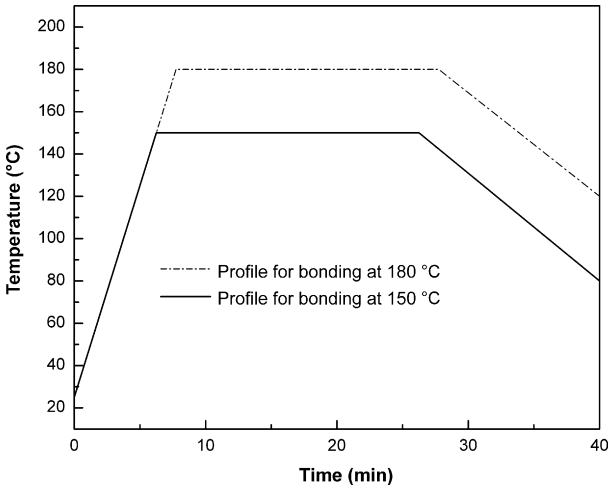

Fig. 2. Bonding temperature profiles.

was done by using dry film as a photoresist material. Ti–Cu–Ni–Au metallization was sputtered on $Si/SiO_2/SiN$ substrate with the thickness of 0.05, 2, 0.05, and 0.03 μm, respectively. Here thin Ti layer acted as the adhesive layer, and Ni was the buffer layer for bonding process. A thin Au layer was necessary for wetting and to prevent metals from oxidation before solder deposition. Four alternatives Sn/In solder layers with the thickness of 1, 1, 0.8, and 0.7 μm were deposited in turn by e-beam evaporation. A near eutectic compositions of InSn alloy would be achieved according to the thickness ratio between In and Sn. To protect solder surfaces from getting oxidized, a 0.03 μm thick Au layer was deposited on the top. After deposition and dry film stripping, O_2 plasma descum was conducted before the bonding process to remove the oxide layer and organic contaminants to obtain a clean surface. Two wafers with the same structure were bonded face to face using wafer bonder (EVG 520) in controlled N_2 atmosphere. In the present case, bonding pressure was 5.50 MPa and bonding temperature was 180 or 150 °C. As shown in Fig. 2, the bonding time was 20 min at peak temperature. After bonding, the bonded wafers were diced into dies with size of 13 mm × 13 mm with a dicing speed of 2 mm/s.

2.2. Characterization of the seal joints after bonding

After dicing, all the dies were checked by cross-section scanning acoustic microscopy (C-SAM) for non-destructive study of the bonding interface. The process involved launching ultrasonic waves into the samples at a frequency of 230 MHz using a piezoelectric transducer. 5 samples for each bonding temperatures were mounted and cross-sectioned for scanning electron microscopy (SEM) observation. These samples were grinded with SiC paper, and polished with 1.0 μm diamond and 0.05 μm silica suspensions. Energy dispersive X-ray (EDX) analysis was used to study the compositions of the bonded ring joints. Focus ion beam (FIB) was employed to prepare thin film for transmission electron microscopy (TEM) and EDX examination of the joint.

The hermeticity of the ring seals for patterned dies was evaluated by helium leak rate tests based on MIL-STD-883 [26]. According to the internal cavity volume of the bonded dies (~0.02 cm^3), the pressure of helium gas in bombing chamber was set as 0.5 MPa (75 Psi), and exposure time was 2 h. After bombing, the dies were put into helium leak detector to measure the leak rates. 20 bonded dies were tested. To evaluate the mechanical properties of the seal ring joints, 5 samples were used for shear tests. The shear test was conducted with a shear tester (BT4000 Dage) using a speed of 50 μm/s.

2.3. Reliability study of the seal joints

Reliability tests of the boned dies were studied in detail. Pressure cooker test was conducted under 121 °C, 2 atm for 300 h. High humidity storage was done at 85 °C, 85 RH for 1000 h. High temperature storage test at 125 °C and temperature cycling test (−45 to 125 °C) up to 1000 h were also performed. 21 samples were used for each test. After tests, these dies were examined by C-SAM, helium leak rate and shear tests again.

3. Results and discussion

3.1. Interfacial microstructure after materials deposition

The interfacial microstructure and morphology of the faying surfaces are very important for bonding process. The cross-sectional

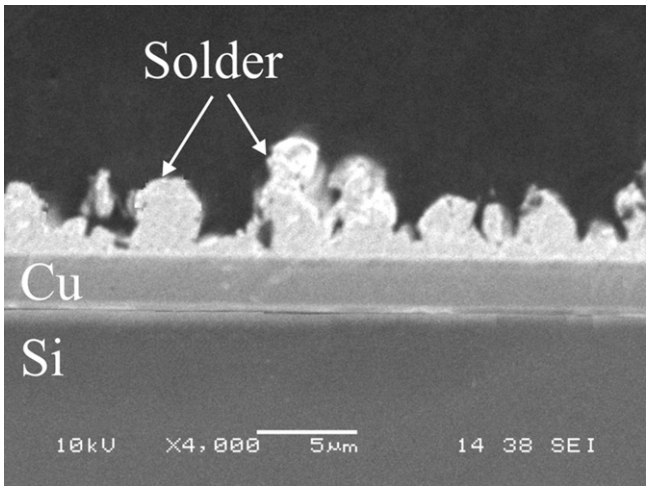

Fig. 3. SEM image of the interface microstructure after materials deposition.

interface of the as-received solder/metallization after deposition was examined by SEM, as shown in Fig. 3. According to the EDX analysis, no Cu was found inside of solder matrix which meant thin Ni buffer layer was effective to prevent Cu diffusion. The solder composition was ~60% (atom percentage, hereafter) Sn, ~40% In and a trace mount of Au. From this image, we found that after In/Sn layers deposition, the grains with size of ~3 μm were formed and they were surrounded by deep channels. The formation of such non-planar solder layer was due to the surface properties of the two materials. It has been reported that the surfaces of In film after deposition at room temperature, grains were separated by deep channels, and the surfaces of Sn films had grains separated by occasional deep voids [27]. The atomic force microscope (AFM) analysis on a 20 μm × 20 μm area of the surface was carried. The roughness analysis was performed on the cut surface of 500 nm height away from the bottom of the surface. The 3-D image of the cut surface was shown in Fig. 4 and the roughness of this cut surface was about 400 nm. For such a non-planar surface, more oxides would form since it had a larger surface area. Higher bonding force was preferred to destroy the oxide film and let the liquid solder fill up the gaps between the asperities.

3.2. Bonding yield with C-SAM examination

We screened the bonded dies after dicing by using C-SAM (Cross-section Scanning Acoustic Microscopy). A die was defined as a "good die" if there were no detectable voids and/or cracks under C-SAM. The bonding yield was further defined as the percentage of good dies to the gross dies of a bonded wafer. According to C-SAM scanning images of the bonded wafers, there were no detectable voids in any single seal ring produced both under 180 and 150 °C. That meant a 100% yield after bonding was achieved by present bonding method. The typical C-SAM graph of dies bonded at 180 and 150 °C

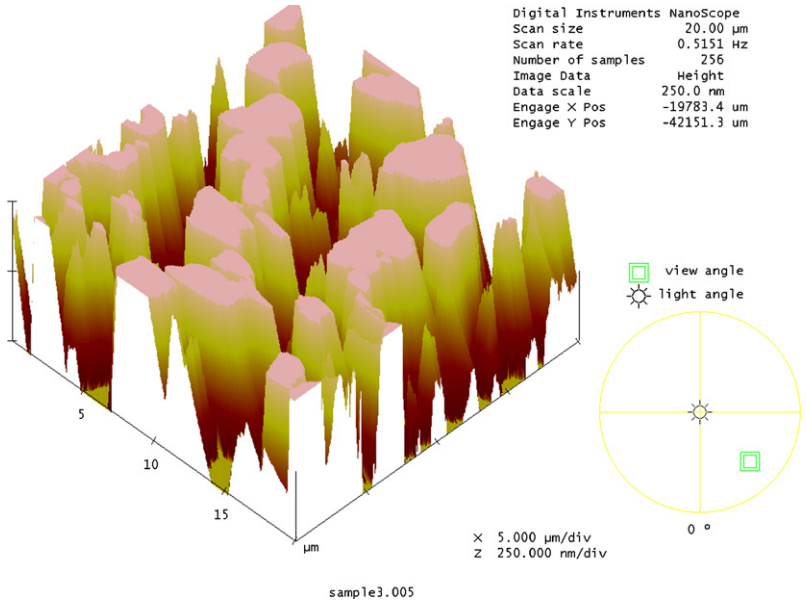

Fig. 4. AFM image of the surface morphology.

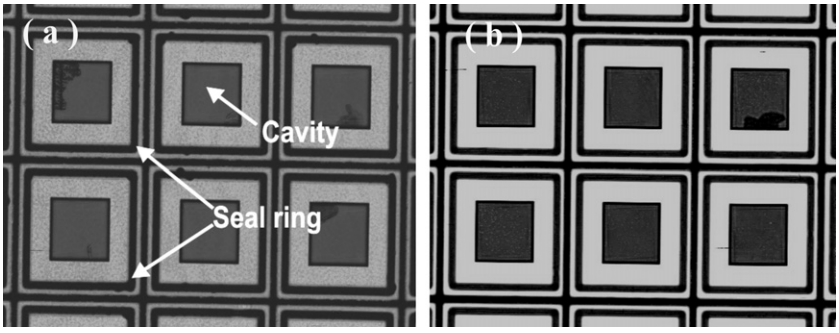

Fig. 5. C-SAM graphs of devices bonded at (a) 180 °C and (b) 150 °C.

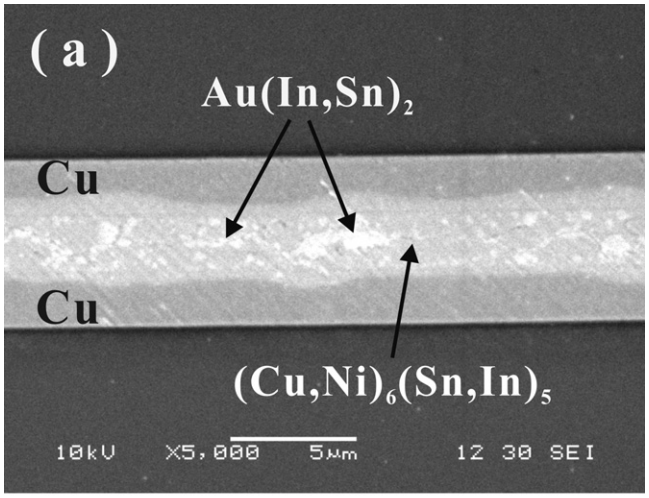

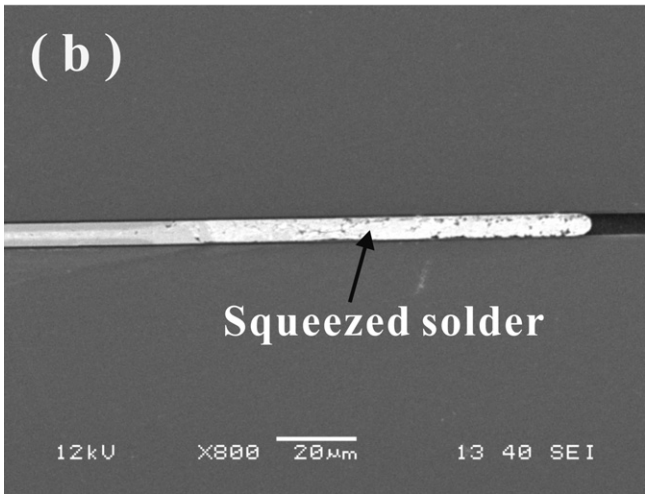

Fig. 6. Interfacial microstructure of the seal joint bonding at 180 °C: (a) at the center region; (b) at the side region.

were shown in Fig. 5(a) and (b). It was clear that each bonding ring was in a uniform gray color indicating the bonded joints had intimate contact. Here we need point out that the resolution of C-SAM is about several microns and small voids cannot be detected.

3.3. Microstructure of seal rings under different bonding temperature

The interfacial microstructures showed that voids free joints were obtained after bonding at 180 °C. As shown in Fig. 6(a), remaining Cu and a thin IMC layer were formed in the joint. Two kinds of IMCs were detected by EDX. The composition (at.%) of the main phase in gray color is Cu:Ni:Sn:In = 43–56:5.77–11.30:25–35:9–25. The atom ratio between (Cu,Ni) and (SnIn) was 53–61:47–39. As shown in Fig. 7, according to the thermodynamic calculation of phase equilibrium in Cu–In–Sn system at 180 °C [28], a η phase existed in the system. It was known that η phase existed in both the two binary systems, i.e., η-Cu_2In in Cu–In and η-Cu_6Sn_5 in Cu–Sn [28]. Sommadossi et al. had found the existence of the two phases in the Cu/In–48Sn/Cu joint produced by annealing at 220 °C for 436 h [29]. In our case, the detected composition agreed very well with that of η-$Cu_6(Sn,In)_5$. Since Ni can easily diffuse into η-Cu_6Sn_5, $(Cu,Ni)_6(Sn,In)_5$ phase was finally obtained. Another particle compounds embedded in η phase with white color were Au rich phase. According to the TEM/EDX result, it was confirmed as

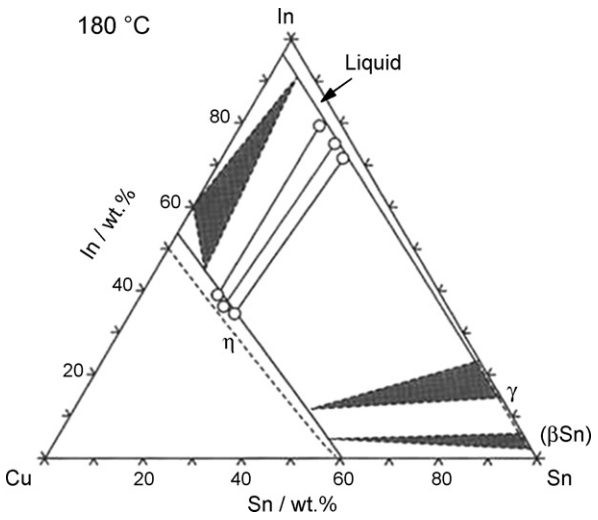

Fig. 7. Isothermal section of Cu–In–Sn system at 180 °C [28].

$Au(In,Sn)_2$ phase. For the present materials design, the thickness of seal joint should be around 10 μm. However, the achieved thickness value was about 7 μm. The reason is that under present bonding temperature, solder materials melt fast and had a good flowability. When bonding pressure was applied, a portion of liquid alloy was squeezed out. As shown in Fig. 6(b), the length of the squeezed solders was about 80 μm.

Detail microstructure was revealed by TEM. Fig. 8(a) showed the cross-sectional microstructure at the Si/Cu interface. The thicknesses of SiO_2, SiN and Ti were consistence with the design. Fig. 8(b) showed the cross-sectional microstructure of the region of Cu/IMCs. EDX result was listed in Table 1. It was found that the phase adjacent to Cu component was $Cu_6(Sn,In)_5$, and next was $(Cu,Ni)_6(Sn,In)_5$. Island shape $Au(In,Sn)_2$ phases embedded in the $(Cu,Ni)_6(Sn,In)_5$ phase were also determined. These results confirmed that after bonding, Ni buffer layer has been dissolved into $(Cu,Ni)_6(Sn,In)_5$ phase. The content of Ni in this quaternary phase can reach 11.7 at.%. The soldering bonding process involving buffer layer can be explained as followed. At beginning, liquid solder alloy would form at the bonding temperature owing to the slow reaction between solder and Ni buffer layer [30]. Then liquid solder started to react with Ni layer. According to the studies of the interfacial reactions between liquid In–49Sn solder and Ni, Ni would dissolve into liquid solder as either Ni_3Sn_4 [31] or NiInSn phase [32]. Because Ni buffer layer is very thin, this process would be quite short. In the next phase, InSn solder began to react with Cu to form $Cu_6(Sn,In)_5$ compounds. Since Ni has a large solubility in the $Cu_6(Sn,In)_5$ compounds, chemical potential gradient led the dissolution of the Ni containing compounds. As a result, all Ni atoms went into $Cu_6(Sn,In)_5$ solution.

As shown in Fig. 9(a), when bonding at 150 °C, the interface was composed of three parts: residue Cu, $(Cu,Ni)_6(Sn,In)_5$ and

Table 1
EDX analysis along the interface shown in the TEM image.

Point	Element (at.%)					Equilibrium phase
	Cu	Ni	Sn	In	Au	
1	100					Cu
2	47.4		35.4	17.2		η-$Cu_6(Sn,In)_5$
3	32.6	8	43.2	16.2		η-$(Cu,Ni)_6(Sn,In)_5$
4	36.5	11.7	45	6.8		η-$(Cu,Ni)_6(Sn,In)_5$
5	5.7		6	55.1	33.3	$Au(In,Sn)_2$
6	11.6		13.2	47.6	27.7	$Au(In,Sn)_2$
7	42.6	6	41.8	9.6		η-$(Cu,Ni)_6(Sn,In)_5$

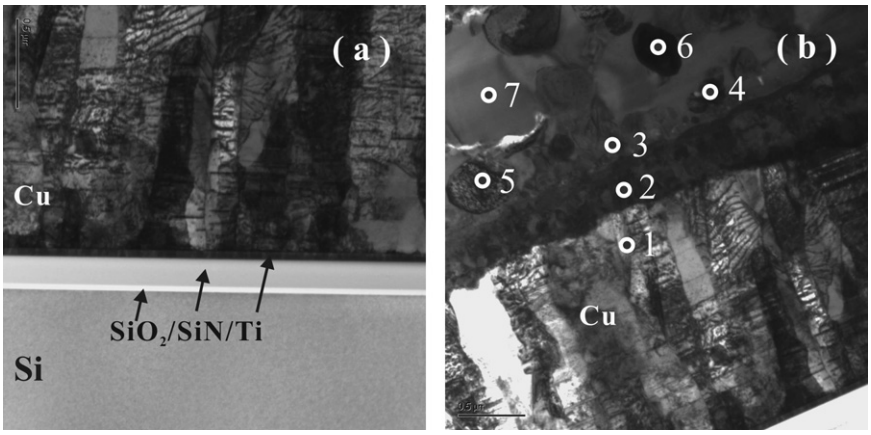

Fig. 8. TEM images of bonding microstructure: (a) at Si/Cu interface region; (b) at the Cu/IMCs interface region.

small $Au(In,Sn)_2$ dots located at the middle of the interface. For the $(Cu,Ni)_6(Sn,In)_5$, the atom percentage of (Cu,Ni): (Sn,In) was 54–60:46–40 which was nearly the same with that formed at the bonding temperature of 180 °C. Continuous threadlike cracks were found at the center of the joint, which would be harmful to the hermeticity and reliability properties. As shown in Fig. 9(b), the length of the overflowed solder was about 20 μm which was smaller than that formed under 180 °C. Comparing with Figs. 6(a) and 9(a), we can also find the thickness of the joint formed at 180 °C is about 7 μm which was thinner than that formed at 150 °C with a thickness of 8 μm. The differences of the two seal joints formed were caused by the different bonding temperatures. At higher temperature, solder material melt fast and has a good flowability. Under the same pressure, a portion of liquid alloy is squeezed out. So thin solder joint was formed with a thin IMC layer at the center part.

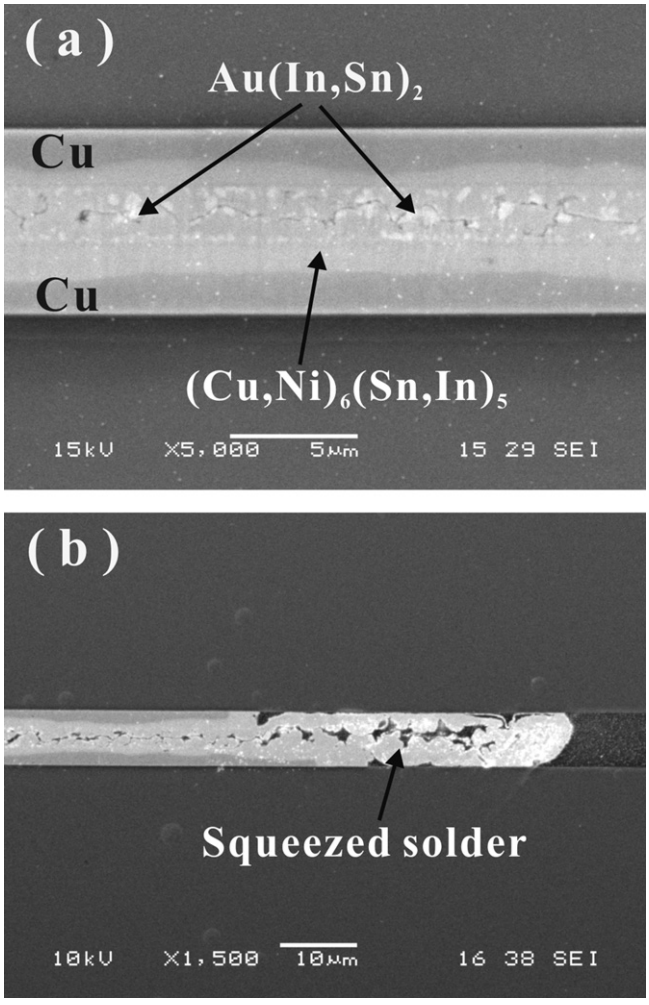

Fig. 9. Interfacial microstructure of the joint bonding at 150 °C: (a) at the center region; (b) at the side region.

The possible reasons for the cracks formation at lower bonding temperature were explained as following. It has been assumed that oxides on materials surface would be trapped within the liquid phase and pushed forward by the advancing solid–liquid boundaries in diffusion bonding for Al alloys using Cu interlayer [33]. These oxide particles agglomerated at the bond line and prevented metal-to-metal contact from being established fully. In our case, although O_2 plasma descum was conducted on the surface, thin oxide film would exist. In addition, as aforementioned, at the surface of the solder materials, one thin AuIn layer would be formed after thin Au layer deposition. Therefore, in order to form a good seal joint, during bonding liquid solders form both bonding pairs must break through oxide film and IMC layer to meet each other. According to the EDX analysis of the solder material before bonding, part of the solder may not even melt at the bonding temperature of 150 °C. The flowability of liquid solder and the wetting property were also poorer comparing with that under high bonding temperature. Larger fragments of oxide film and IMCs existed at the interface. As the liquid solidified isothermally due to continued inter-diffusion, solid/liquid interfaces will push the fragments of oxide and IMCs towards to the center region, where they agglomerated. Due to the poor wetting between IMCs and oxides, cracks were formed at the place where they were rich. As a contrast, when bonding at 180 °C, the temperature difference was larger. The better flowability would help the oxide film and IMCs break up into small fragments, in which it increased the difficulty of the formation of continuity of oxides and IMCs at the bonding line during solidification. Koyama et al. had found continuous Sn oxides formed at a lower diffusion temperature which later became discontinuous as the bonding temperature was increased [34]. As a result, no detectable cracks formed at the bonding interface.

3.4. Hermeticity and shear strength of the seal rings

Helium rate test was performed to examine the hermeticity of the seal. 21 bonded dies were tested. The results show that the leak rate of the devices bonded at 180 °C is smaller than 5×10^{-8} atm cm^3/s, which is the rejected limit value of MIL-STD-883E. However, for the devices bonded at 150 °C, only 52% devices have leak rate smaller than 5×10^{-8} atm cm^3/s. The average shear

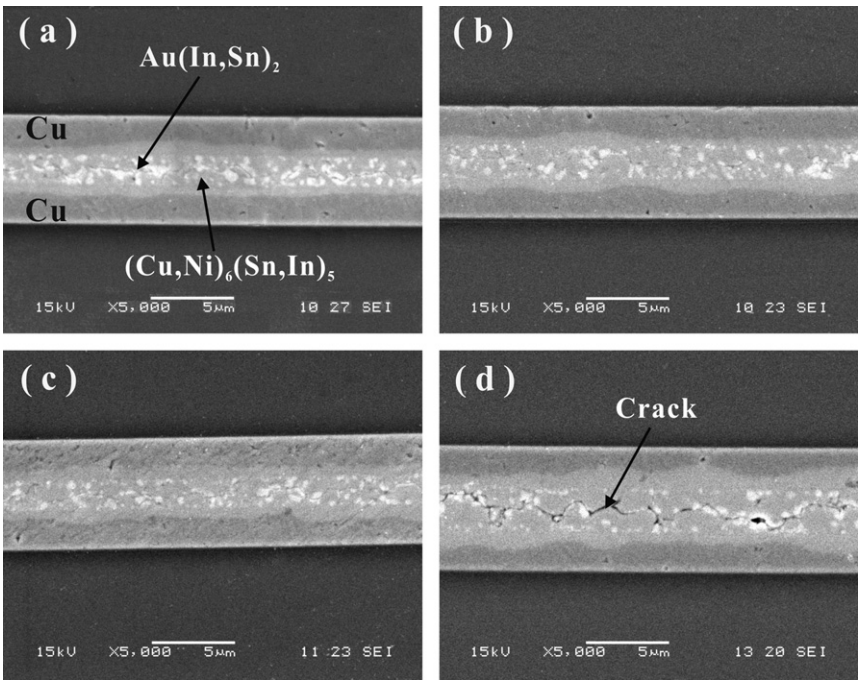

Fig. 10. Interfacial microstructure of seal joint of good dies after reliability tests: (a) pressure cooker test; (b) high humidity storage; (c) high temperature storage; (d) temperature cycling.

strength of the joints formed at 180 °C is 32 MPa, and that is 26.70 MPa for the joints formed at 150 °C. Since there is no voids and the $Au(In,Sn)_2$ phase is not continuously, both the shear strength and hermeticity properties will be improved comparing with the seal formed at 150 °C.

3.5. Reliability properties of the seal rings

Since the hermeciticy of the dies bonding at 150 °C was not very good, for reliability study, only dies bonded at 180 °C were used for reliability evaluation. The results of reliability tests were listed in Table 2. The numbers of the failed dies (leak rate larger than 5×10^{-8} atm cm^3/s) after pressure cooker test, high humidity storage, high temperature storage and temperature cycling were 6, 2, 4, 4 respectively. That meant the ratios of good dies after tests were 71.4%, 90.5%, 81%, and 81%, respectively. At the same time after reliability test, the seal rings with good hermeticity still maintained good mechanical properties. The shear after pressure cooker test, high humidity storage, high temperature storage and temperature cycling were 27.08, 15.37, 12.32, and 16.71 MPa, respectively.

The interfacial microstructures after reliability tests were analyzed. With SEM/EDX analysis, the compositions of the seal joints also have no detectable change. The results were reasonable since the temperatures for reliability tests were not very high comparing with the melting temperatures of the IMC joints. As shown in Fig. 10, it seemed $Au(In,Sn)_2$ compounds slightly grew up during tests comparing with after bonding. According to the shear tests, we believe that the adhesion between different IMCs at the bonding line decreased after reliability tests. Further, as shown in Fig. 10(d), in some samples, we found small cracks along the bonding line.

Samples with poor hermeticity were analyzed to know the failure mechanism of the seal joints. Consistent failure mode was confirmed. As shown in Fig. 11, big crack throughout the seal joint was found. It is clear that the crack expanded along the bonding line and between $Au(In,Sn)_2$ compounds and $(Cu,Ni)_6(Sn,In)_5$ compounds. We have discussed before that at the bonding line, thin oxides would exist after bonding. With the existence of different IMCs at the interface, under thermal cycling and pressure cooker tests, stress would generate along the bonding line which would lead the formation and propagation of cracks. This was the reason why after these two tests, the leak rate test revealed a relative poor hermeticity results comparing with other tests. When the samples with voids or cracks were put inside the bombing chamber, under the pressure of 75 Psi, large number of helium atoms would be pushed into the cavity inside the seal ring, which would

Table 2
The result of long-term reliability test.

Reliability test items	Number of failed samples Leak rate test (total number of samples = 21)
Pressure cooker test	6 (=28.5%)
High humidity	2 (=9.5%)
High temperature storage	4 (=19%)
Temperature cycle	4 (=19%)

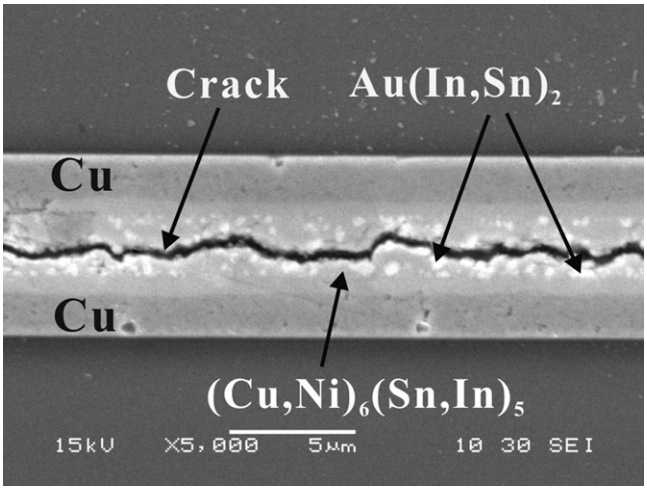

Fig. 11. Interfacial microstructure of the failed seal joint after PCT test.

cause further damage of the seal ring. Reliability results indicated that the adhesion between IMCs, IMCs and oxides were the key to determine the reliability of the seal joint. Therefore, two ways can be used to further improve the reliability of the present bonding seal joints. One is to reduce volume ratio between $Au(In,Sn)_2$ and $(Cu,Ni)_6(Sn,In)_5$ compounds by thin Au layer and/or thicker solder deposition which will result in discontinuous Au rich phase formation. The other way is to reduce surface oxides by optimizing the plasma treatment process.

4. Conclusions

Low cost and high yield wafer-to-wafer bonding using In/Sn solder and Cu/Ni/Au metallization system was investigated. Various tests were conducted to evaluate the reliability properties of the bonded devices. Some important results are summarized in the followings.

(1) Thin Ni buffer layer effectively prevented the fast diffusion between LMP solder and HMP component. Therefore, 100% yield of good bonding dies was achieved when checked with C-SAM for the two bonding temperatures, i.e., 180 and 150 °C with a bonding pressure of 5.5 MPa.
(2) When bonding at 180 °C, voids free joint composed of η phase and embedded $Au(In,Sn)_2$ IMCs. All samples obtained good leak rate ($<5 \times 10^{-8}$ atm cm^3/s).
(3) When bonding at 150 °C, η-$(Cu,Ni)_6(Sn,In)_5$ and $Au(In,Sn)_2$ IMCs were formed at the joint. Cracks along bonding line were formed due to the poor flowability of liquid solder, which caused poor hermeticity of the seal ring.
(4) After bonding, high shear strength was obtained for the seal rings formed under both bonding temperatures.
(5) The percentage of good dies with the acceptable hermeticity (leak rate smaller than 5×10^{-8} atm cm^3/s) after pressure cooker test, high humidity storage, high temperature storage and temperature cycling were 71.4%, 90.5%, 81%, and 81%, respectively. The propagation of crack along bonding line was found in the failed dies after reliability tests. It was believed that the formation of two different IMCs as well as the agglomeration of oxides at the bonding line weakened the IMC joint. During reliability test, the thermal and/or mechanical stress would accelerate the generation and propagation of the cracks.

Acknowledgements

Chengkuo Lee, PI of IME Core Project 06-420004, would like to thank the Institute of Microelectronics, Agency for Science, Technology and Research (A*STAR), Singapore, for supporting this research.

References

[1] D. Sparks, G. Queen, R. Weston, G. Woodward, M. Putty, L. Jordan, S. Zarabadi, K. Jayakar, J. Micromech. Microeng. 11 (2001) 630–634.
[2] R. Gooch, T. Schimert, MRS Bull. 28 (2003) 55–59.
[3] M.M.V. Taklo, P. Storas, K. Schjolberg-Henriksen, H.K. Hasting, H. Jakobsen, J. Micromech. Microeng. 14 (2004) 884–890.
[4] J. Chae, J.M. Giachino, K. Najafi, J. Microelectromech. Syst. 17 (2008) 193–200.
[5] V. Dragoi, G. Mittendorfer, C. Thanner, P. Lindner, Microsyst. Technol. 14 (2008) 509–515.
[6] P.H. Chen, C.L. Lin, C.Y. Liu, Appl. Phys. Lett. 90 (2007) 132120.
[7] M. Esashi, J. Micromech. Microeng. 18 (2008) 073001.
[8] Q. Wang, K. Jung, M. Choi, W. Kim, S. Ham, B. Jeong, C. Moon, Proceedings of the 7th International Conference on Electronics Packaging Technology, China Electronic Packaging Society, Shanghai, China, 2006, pp. 1–5.
[9] H. Takagi, K. Kikuchi, R. Maeda, T.R. Chung, T. Suga, Appl. Phys. Lett. 68 (16) (1996) 2222–2224.
[10] T. Chung, N. Hosoda, T. Suga, H. Takagi, Appl. Phys. Lett. 72 (13) (1998) 1565–1566.
[11] F. Niklaus, H. Andersson, P. Enoksson, G. Stemme, Sens. Actuators A Phys. 92 (2001) 235–241.
[12] Q. Wang, S.H. Choa, W.B. Kim, J.S. Hwang, S.J. Ham, C.Y. Moon, J. Electron. Mater. 35 (3) (2006) 425–431.
[13] L.L. Yan, C.K. Lee, D.-Q. Yu, A.B. Yu, W.K. Choi, John H. Lau, J. Electron. Mater. 38 (1) (2009) 200–207.
[14] C. Lee, A. Yu, L.L. Yan, H. Wang, J.H. He, Q.X. Zhang, John H. Lau, Sens. Actuators A, in press, doi:10.1016/j.sna.2008.10.011.
[15] C.C. Lee, Y.-C. Chen, G. Matijasevic, IEEE Trans. Comp. Packaging Manuf. Technol. 16 (1993) 311.
[16] Y.-C. Chen, C.C. Lee, Thin Solid Films 283 (1996) 243–246.
[17] Y.-C. Chen, W.W. So, C.C. Lee, IEEE Trans. Comp. Packaging Manuf. Technol. A 20 (1997) 46.
[18] C. Lee, J.-S. Shie, W.-F. Huang, Sens. Actuators A 85 (2000) 330–334.
[19] R.W. Chuang, C.C. Lee, IEEE Trans. Comp. Packaging Technol. 25 (2002) 453.
[20] O. Brand, H. Baltes, Microsensor packaging, Microsyst. Technol. 7 (2002) 205–208.
[21] Riko I. Made, C.L. Gan, L.L. Yan, A. Yu, S.U. Yoon, J.H. Lau, C. Lee, J. Electron. Mater. 38 (2009) 365–371.
[22] C.C. Lee, S. Choe, Mater. Sci. Eng. A 333 (2002) 45–50.
[23] D.-Q. Yu, C. Lee, L.L. Yan, W.K. Choi, A. Yu, John H. Lau, Appl. Phys. Lett. 94 (2009) 034105.
[24] K. Sakuma et al., Proceedings of the 58 Electronic Components and Technology Conference, Orlando, Florida, 2007, pp. 627–632.
[25] T. Studnitzky, R. Schmid-Fetzer, JOM 54 (12) (2002) 58–63.
[26] MIL-STD-883E, method 1014.10, 14 March 1995.
[27] M. Higo, K. Fujita, Y. Tanaka, M. Mitsushio, T. Yoshidome, Appl. Surf. Sci. 252 (2006) 5083–5099.
[28] X.J. Liu, H.S. Liu, I. Ohnuma, R. Kainuma, K. Ishida, S. Itabashi, K. Kameda, K. Yamaguchi, J. Electron. Mater. 30 (9) (2001) 1093–1103.
[29] S. Sommadossi, A. Fernandez Guillermet, Intermetallics 15 (2007) 912–917.
[30] J.F. Li, S.H. Mannan, M.P. Clode, Scr. Mater. 54 (2006), 1773-1778.
[31] C.-Y. Huang, S.W. Chen, J. Electron. Mater. 31 (2) (2002) 152–160.
[32] S.S. Wang, Y.H. Tseng, T.H. Chuang, J. Electron. Mater. 35 (1) (2006) 165–169.
[33] S. Koyama, M. Takahashi, K. Ikeuchi, Solid State Ionics 172 (2004) 397–401.
[34] A.A. Shirzadi, H. Assadi, E.R. Wallach, Surf. Interface Anal. 31 (2001) 609–618.